



Folding behavior of thermoplastic hinges fabricated with polymer extrusion additive manufacturing

Cesar Omar Balderrama-Armendariz^{1,2} · Eric MacDonald³ · David A. Roberson⁴ · Leopoldo Ruiz-Huerta^{2,5} · Aide Maldonado-Macias⁶ · Esdras Valadez-Gutierrez¹ · Alberto Caballero-Ruiz^{2,5} · David Espalin⁷

Received: 24 April 2019 / Accepted: 23 July 2019
© Springer-Verlag London Ltd., part of Springer Nature 2019

Abstract

Due to the layer-by-layer nature of additive manufacturing, fabricated parts suffer from an anisotropic behavior with reduced mechanical performance when compared to traditional manufacturing. One specific mechanical property, folding endurance, requires both low flexural strength and simultaneously high elongation to achieve the flexibility needed to sustain repetitive bending. The present work provides an analysis of selected thermoplastics' flexural capacity, including nylon (PA), polyethylene terephthalate (PETG), polylactide (PLA), thermoplastic polyurethane (TPU), polypropylene (PP), polyethylene (PE), and a TPR blend (ABSMG94: SEBS-g-MA 25:75), in order to evaluate the maximum number of folding cycles and load capacity sustained by a living hinge. A fractographic analysis was performed using scanning electron microscopy and computed tomography. Similar to the performance of injected molded products, the experimental results demonstrated that three of the tested materials behaved well in the context of a large number of folding cycles prior to an eventual detachment into two pieces; TPR blend, 244,424 cycles; PP endured one million cycles; and TPU, more than two million cycles, while the remaining materials failed to survive more than 1000 cycles. The hinges failure analysis revealed a wide variety of fracture morphologies and failure modes. In regard to the load capacity, PLA, PETG, and nylon provided the highest results in the ultimate strength of an axial static force applied (790.61 N, 656.06 N, and 652.75 N respectively), while the TPR blend was the highest (398.44 N) of the elastomeric materials (PP, TPU, and TPR blend). The evaluated materials demonstrated enough flexibility for use in specific applications such as stretchable electronics and wearable applications.

Keywords Polymer extrusion · Additive manufacturing · Folding endurance · Flexible 3D printed materials · Flexible Applications · Fused deposition

✉ Cesar Omar Balderrama-Armendariz
cesar.balderrama@uacj.mx

Eric MacDonald
ewmacdonald@ysu.edu

David A. Roberson
droberson@utep.edu

Leopoldo Ruiz-Huerta
leopoldo.ruiz@icat.unam.mx

Aide Maldonado-Macias
amaldona@uacj.mx

Esdras Valadez-Gutierrez
esdras.valadez@uacj.mx

Alberto Caballero-Ruiz
alberto.caballero@icat.unam.mx

David Espalin
despalin@utep.edu

¹ Rapid Prototyping Laboratory, Universidad Autónoma de Ciudad Juárez, 32310 Ciudad Juarez, Chihuahua, Mexico

² National Laboratory for Additive and Digital Manufacturing (MADiT), 04700 Mexico, Mexico

³ Advanced Manufacturing Research Center, Youngstown State University, Youngstown, OH 44455, USA

⁴ Polymer Extrusion Lab, The University of Texas at El Paso, El Paso, TX 79968, USA

⁵ Instituto de Ciencias Aplicadas y Tecnología, Universidad Nacional Autónoma de México, 04700 Cd. Mx., Mexico

⁶ Department of Industrial and Manufacturing Engineering, Universidad Autónoma de Ciudad Juárez, Chihuahua, Mexico

⁷ W. M. Keck Center for 3D Innovation, The University of Texas at El Paso, El Paso, TX 79968, USA

1 Introduction

Additive manufacturing (AM) continues to impact society with new applications in the biomedical, automotive, pharmaceutical, and aerospace industries—particularly as material options become more diverse in terms of mechanical properties. Physically flexible materials for AM are now becoming available and are employed to develop novel textile patterns unachievable by conventional textile processes [1–3]. Personalization advances as anthropometric data acquired from anatomy scanning is translated into wearable consumer-specific AM-fabricated products such as clothes or footwear [4]. Important companies such as Adidas, Under Armour, or Nike now offer athletic shoes manufactured with the use of different 3D printing technologies.

While *stiff* 3D printing electronics are transforming the way satellites and other aerospace components are made [5], *flexible and stretchable* 3D printing electronics are now also garnering attention in order to produce conformal formats that are difficult or impossible to achieve through traditional PCB manufacturing technologies. Today, strain sensors can be printed within highly stretchable elastomers [6], and nanotube-integrated circuits can be printed on flexible plastic substrates [7]. Furthermore, the advancements in 3D techniques (e.g., the inclusion of nanoparticle deposition, for example) are enabling environmentally friendly and cost-effective, large-area flexible electronics processes [8], and high-performance integrated electronics that can incorporate any combination of semiconductors and nanomaterials can now be manufactured in either rigid or flexible device substrates [3, 9].

The research topic of flexible 3D printing electronics is broad and expanding. New business models are being explored to allow for unprecedented customization in the production of flexible orthoses with embedded sensors [10], flexible inserts in finger articulations of robotic hands [11], soft robots that exploit novel amorphous, non-rigid dynamics [12] using embedded shape memory alloy coils [13], 3D printing dielectric elastomer actuators [14], and pneumatic/internal combustion systems to generate a jumping movement through a flexible body [15]. Many of these applications are enabled by improvements in the folding properties of printable materials, requiring a rigorous characterization of each in terms of endurance and load.

AM processes and materials for flexible applications must be selected according to characteristics of the final printed part. Polymer extrusion printing is based on the original fused deposition modeling (FDM™), the line of Stratasys production systems, and is now the most commonly used AM technology. Low-cost polymer extrusion machines, along with the diverse variety of available filaments, facilitates new possibilities for (1) personalized products unique to each customer; (2) complex, not previously manufacturable geometries; and (3) the avoidance of assembly by consolidating components.

Significant previous work has explored measuring the mechanical properties given the anisotropic behavior of the performance including: mechanical tensile strength [16–21], compressive strength [20, 22, 23], flexure force [23–25], impact [19, 25, 26], and torsion [27, 28]. However, the characterization of flexural endurance in which test structures are subjected to repetitive folding cycles is largely absent in the literature for 3D printing flexible materials.

Folding endurance is defined as the number of folds required to make a test piece break under standardized conditions [29]. Standard test methods apply for the characterization of paper, and the process is well modeled [29, 30], yet there are no specific formulas or standards to evaluate the maximum folding cycles for polymers. In addition, material suppliers fail to provide associated information in their products' datasheets. Traditional injection molding materials such as PP are common used in living hinges. PP is a material that can surpass one million folding cycles [31] with a maximum load of up to 137.89 kPa [32]. Other available injection molding materials include polyvinyl chloride (PVC), urethane, and PETG provided by suppliers such as San Diego Plastics, Inc. (San Diego, CA, USA). This paper aims to characterize many of these recently commercially available 3D printable materials with regard to their flexibility.

2 Experimental process

Seven 3D printing filament materials were selected with varying flexural strength and elongation as required to provide a spectrum of flexibility necessary to optimize applications with high cycle counts of bending. Nylon 12 (Stratasys, Ltd., Eden Prairie, MN, USA), PETG, polylactic acid (PLA), polypropylene (PP) (Gizmo Dorks, Temple City, CA, USA), thermoplastic polyurethane (TPU) Ninjaflex 85A (NinjaTek, Manheim, PA, USA), polyethylene (PE) co-polymer (Taulman 3D-DuPont, MO, USA), and a blend of acrylonitrile butadiene styrene (ABS) and styrene ethylene butylene styrene grafted with maleic anhydride (SEBS-g-MA) first reported by Siqueiros et al. [33] (University of Texas at El Paso, W. M. Keck Center for 3D Innovation, TX, USA). This last material is referred to hereafter as a thermoplastic rubber blend (TPR blend) consisting of 25% (by weight) ABS blended with 75% SEBS-g-MA.

A specific 3D design for flexural test specimens was developed as there are no standard test artifacts to adequately evaluate extruded polymers. Standard test methods in ASTM-D2176-97a [29] and ISO 5626:1993 [30] are applicable for the characterization of paper, including sheets with a thickness of up to 0.25 mm. The stiffness of some polymers and the thickness in the layer-by-layer process, as well as the potential transition heat generated by a folding endurance test, which specifically targets paper, is discarded for 3D printed

structures. Thus, living hinges were considered the best option to perform folding tests to evaluate the performance of 3D printed polymers. The first prototypes were developed according to the recommendations for injection-molded living hinges, using rectangular, circular, and parabolic flexure designs [34–36], but the geometries and dimensions were not achievable due to the limits in the spatial resolution of the polymer extrusion process and to the layer-delamination tendency during the test. Alternatively, the recommendation in the work presented by Smyth [37] to produce living hinges using desktop extrusion printers was selected. A “planar-V” design (Fig. 1) with 1 mm of thickness, an 80° aperture, and 1.5 mm of distance between the sides of the hinge to allow an opening of 180° were used.

Two main tests were selected with the objective of determining the endurance of the 3D printed living hinges: test 1 for folding endurance and test 2 for static axial loads.

2.1 Test 1 folding endurance

A testing station (Fig. 2) was fabricated and controlled by an Arduino UNO (Arduino LLC) with four servomotors (JR ST47BB, Champaign, IL, USA) working at 2.22 cycles per second. Hinges were clasped with holders tightened with screws. The motor rotation center was aligned with the center of the hinge folding area. The controller was programmed to count the servomotors cycles with 180 degrees of rotation, allowing for enough torque to fold hard hinges (514 N/m) and for automatic process interruption when the hinge became fully detached.

In order to obtain the best printing quality, process parameters were optimized for each material, and in some cases, specific materials were printed in different printers depending on material and process interactions: Nylon specimens were printed on Stratasys Fortus 400mc (Stratasys, Ltd., Eden Prairie, MN, USA), and the rubber blend was printed using a Lulzbot Taz 6 (Aleph Objects, Inc., Loveland, CO, USA) as

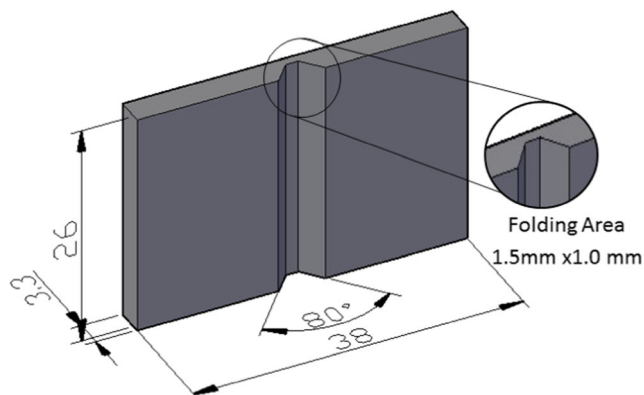


Fig. 1 Living hinge specimen. The function of the two sides of the folding area is to grab specimen during test (Units are in mm.)

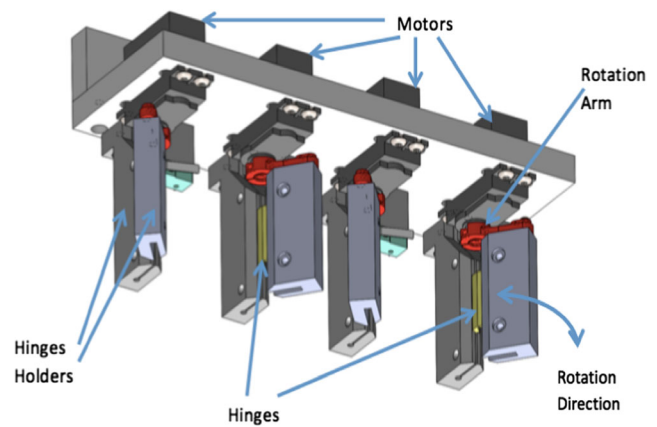


Fig. 2 Control station for folding endurance test

well as other materials with the MakerBot Replicator™ Dual Extruder (MakerBot Industries, Brooklyn, NY, USA). The use of different systems meant that comparisons were more difficult to make, but in general, all extrusion processes were similar enough to render reasonable comparisons. The use of different systems was unavoidable because professional equipment cannot print all flexible materials. To avoid damaging more brittle materials at room temperature, specimens were heated to 80 °C and manually bent ten cycles to provide fiber orientation consistent with the folding motion.

2.2 Test 2 static axial loads

In general, filament manufacturers provide data on physical characteristics in compression, tension, and impact. The present experiment was performed in order to test hinge endurance in the axial direction and to find features that would determine the suitability of the thermoplastic material, according to the load requirements of the hinge application. To evaluate hinge function-associated physical properties, specimens were attached to two axial load test fixtures (Fig. 3). The Static Axial Load Test consisted of measuring pressure with a force gauge (Lutron FG-5100, Lutron Electronic Enterprise Co., Ltd.) applied with a load cell (980 N) in the axial direction. The test is not a standardized evaluation like tension or compression as the folding endurance area is exposed to multidirectional forces. Units of measure are expressed in Newtons, and applied force was measured at two points during the test:

1. During the initial motion, with less than 100 μm of displacement (initial applied force), the objective was to determine the point of endurance prior to the elastic motion that allowed load bearing with no impact on the hinge function.
2. When the specimen reached the ultimate load prior to the break point in order to determine the maximum load that the hinge could endure.

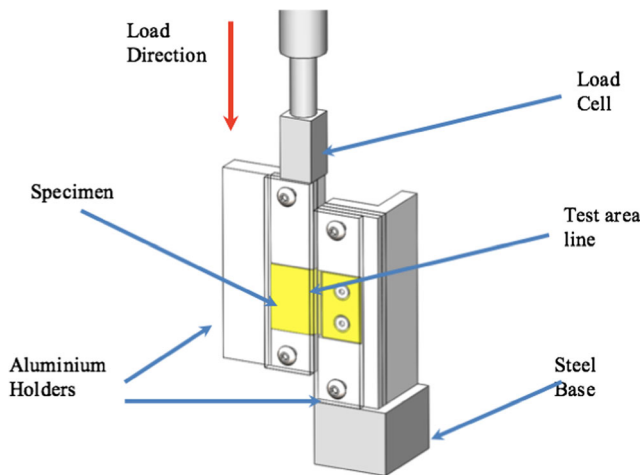


Fig. 3 Static axial load. Load direction is perpendicular to the hinge folding movement

3 Pre-experiment process

To understand the printed parts' anisotropic behavior, a preliminary experiment was performed to find the correct orientation of the printed specimens as well as to identify the appropriate raster angle at which the maximum folding cycles would be obtained. Considering the orthogonal directions presented in the ASTM F2792-12a [38], XYZ and XZY orientations were selected due to improved strength. For the raster, angles at 0°, 90°, and 45°/–45° were also considered. Figure 4 shows hinge orientation viewpoints and raster direction. According to the hinge design, a folding line was defined at the middle of the hinge. For rapid results, PLA specimens were tested with printing parameters deliberately fixed at 0.25 mm of layer thickness with zero air gap, two shells, and 100% of infill. G code was modified in the desktop printers to use raster angles of 0°.

Fig. 4 Representation of the orientation and raster angle on the hinges specimens with initial data of pre-experiment (Values are on the number of folding cycles obtained.)

Build Orientation	Raster Angle	Replicas				
		1	2	3	\bar{x}	s
 XYZ	45°/45°	210	196	185	197.0	12.53
	0°	220	200	205	208.3	10.41
	90°	122	112	109	114.3	6.81
 XZY	45°/45°	97	107	113	105.7	8.08
	0°	140	165	129	144.7	18.45
	90°	56	37	42	45.0	9.85

ANOVA highlighted that both orientation and raster angle are factors which determine the number of folding cycles, with a $p = 0.00$ in both cases. As in the results in Fig. 5, a pairwise comparison between XYZ and XZY showed a difference in these two levels with a $p = 0.00$. When verifying a difference between the three raster angle levels (0°, 90°, and 45°/–45°), the change in the raster angle's direction resulted in a significant difference in strength. The highest values on the pre-experiment took into consideration the XYZ orientation with the 0° raster angle (208.3 ± 10.41 cycles), which was used for the subsequent principal tests.

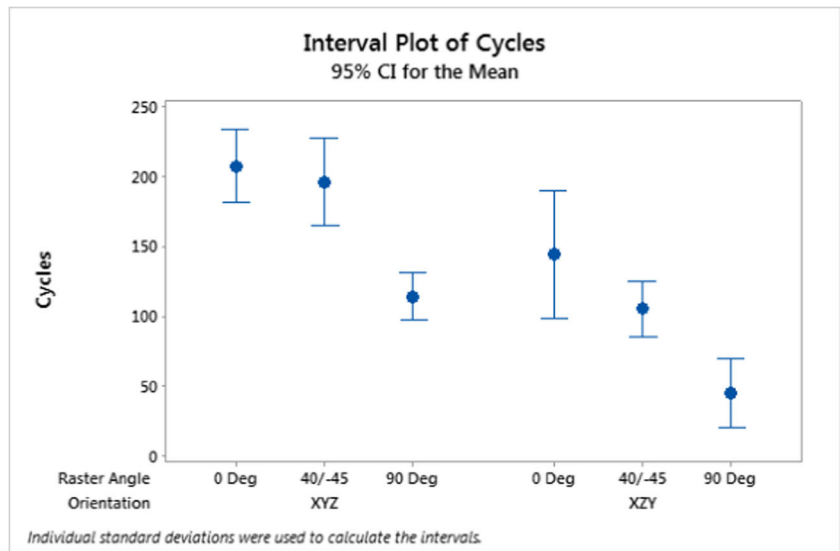
4 Results

4.1 Test 1 folding endurance results

For the folding endurance test, PLA and nylon specimens failed before reaching 200 folding cycles (163.2 ± 29.827 and 198.8 ± 57.246 respectively) and PE and PETG specimens failed before 900 cycles (621.2 ± 112.839 and 856.6 ± 92.578 respectively); thus, the endurance of PLA, nylon, PE, and PETG is considered of low impact for flexible applications due to the low number of folding cycles. The TPR blend presented a reasonable endurance of 244,424 folding cycles; however, both the PP and TPU provided significantly higher endurance. The PP cycles withstood just over one million cycles, and TPU test was interrupted without failure at the test cycle limit of two million cycles. Following the test, the TPU specimens were visually observed, with no damage found on the surface of the folding section.

Paired differences could be observed in the Bonferroni test presented in Fig. 6. This analysis was performed to compare materials and obtain statistical evidence for the folding

Fig. 5 Plot of folding cycles in pre-experiment



endurance results. As observed, PE, nylon, PE, PETG, and PLA showed no significant difference. Despite this lack of variation, PE featured an advantage of more than 600 folding cycles over nylon and PLA. This lack of statistical difference is due to the fact that the folding cycles of PP, and TPU are significantly higher than the other materials.

Figure 7 shows the results of the folding tests among the considered materials with y -axis in logarithmic format. Again, the predominant materials were TPU, PP, and TPR blend, while PLA and nylon were in the low range with less than 200 cycles.

4.2 Test 2 static axial loads results

Axial loads were applied in the parallel direction of the test area line (see Fig. 3). Specimens printed with materials PP, TPU, and the TPR blend showed a visible plastic deformation

on the fracture line at the end of the test (Fig. 8), while the apparently more brittle materials, including PE, PETG, nylon, and PLA, showed very little deformation in printed rasters at the fracture line. Table 1 represents data obtained in the test: (1) the applied force before an elastic movement in the axial direction occurred and (2) the maximum applied force.

4.2.1 Initial applied force

Regarding the force applied before an elastic movement to test hinge functionality (force before 100 μ m in axial direction), the greatest variability was observed in nylon thermoplastic (± 21.94 N), and in the case of TPU, results differed from the overall means with a mean below that of other materials (Fig. 9), requiring only 5.79 ± 2.58 N to move a TPU hinge in the axial direction (see Fig. 3) versus the 67.27 ± 15.77 N of the PETG specimens. Two distinct groups with a significant

Fig. 6 Bonferroni differences analysis in the folding endurance test

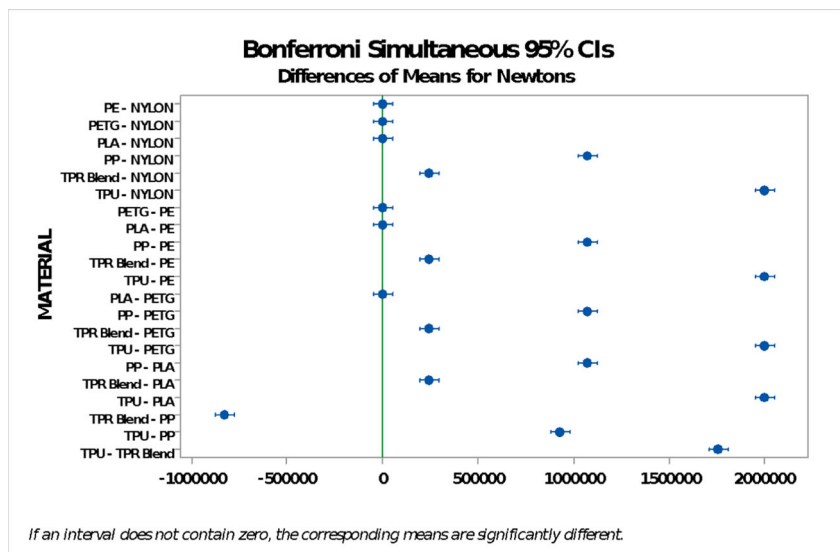
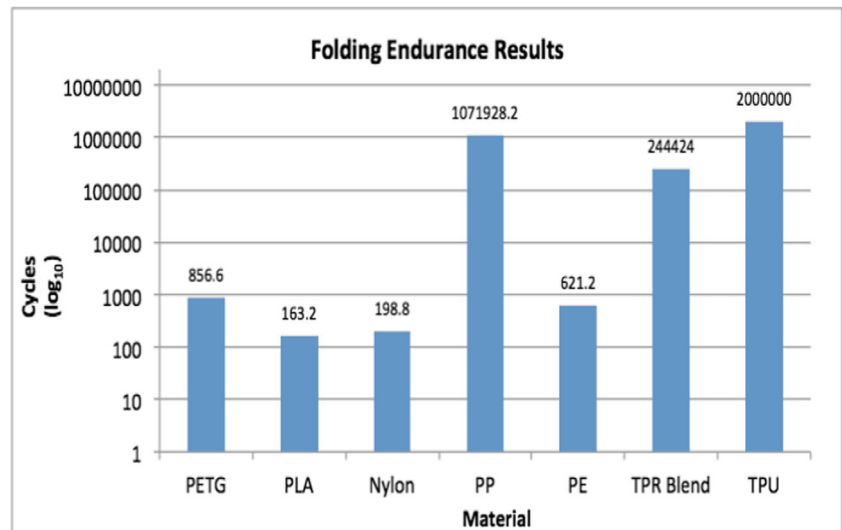


Fig. 7 Comparison of the folding endurance results



difference in endurance were also observed: PE-TPR blend-TPU and nylon-PETG-PLA-PP.

4.2.2 Maximum applied force

PP (293.32 ± 35.05 N) and TPU (267.33 ± 58.92 N) showed no significant differences in the comparison analysis (Fig. 10), and an overlap with individual confidence interval of PETG (656.06 ± 20.47 N) and nylon (652.75 ± 61.09 N) was observed. PLA (790.61 ± 58.46 N) showed the highest level of strength against axial load when compared to the other

materials. Any other paired combination resulted in a significant difference in maximum load (Fig. 11).

Figure 11 shows a comparison of the complete axial test. Although the graph is not a stress-strain graph as the test area on the hinge was exposed to multi-directional forces and the test is not standardized, curves obtained from a force-dimensional relation have been plotted to observe differences. The TPU material curve presented a typical behavior of an elastomer where the elastic/plastic point is difficult to observe reaching the 267.3 N of maximum load (Table 1) and 108 mm of elongation. The TPR blend follows TPU in the elongation

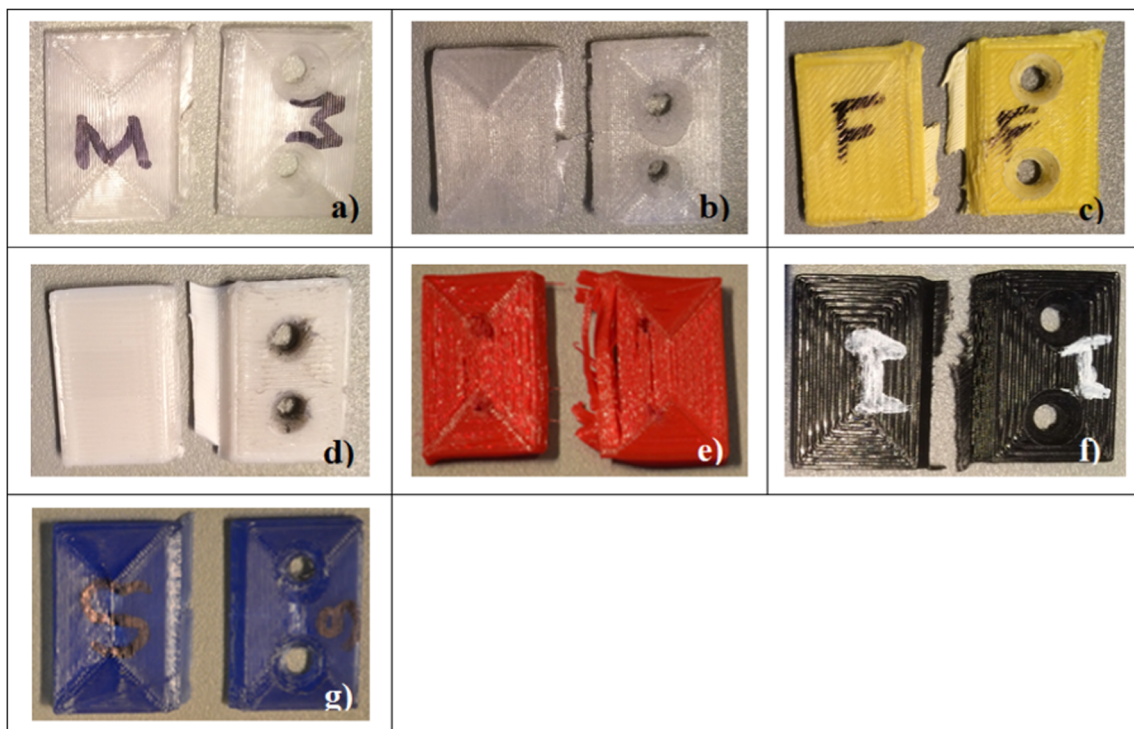


Fig. 8 Differences in the fracture line of considered specimens after the axial load test. Figures are representative of the polymer materials. **a** PE. **b** PETG. **c** PP. **d** TPR blend. **e** TPU. **f** Nylon. **g** PLA

Table 1 Results of axial load test in seven materials at two different points during the test

Specimen	Material																				
	PETG (N)			PLA (N)			Nylon (N)			PP (N)			PE (N)			TPR blend (N)			TPU (N)		
	Before axial move	Maximum load	After axial move	Before axial move	Maximum load	After axial move	Before axial move	Maximum load	After axial move	Before axial move	Maximum load	After axial move	Before axial move	Maximum load	After axial move	Before axial move	Maximum load	After axial move	Before axial move	Maximum load	After axial move
1	84.34	684.99	73.06	688.92	92.18	657.14	36.77	245.66	12.75	452.58	9.81	404.03	10.30	347.16							
2	83.85	657.54	40.21	819.84	41.19	595.26	51.98	268.21	16.18	458.46	10.30	391.29	4.90	235.36							
3	51.98	659.99	79.92	797.28	72.57	614.88	35.30	315.77	15.20	446.20	7.85	380.01	5.39	191.72							
4	61.78	628.12	64.72	811.99	73.06	753.15	50.99	329.50	12.26	438.36	11.77	414.33	4.41	295.18							
5	54.43	649.69	50.99	835.04	42.66	643.32	55.41	307.44	11.28	439.83	8.34	402.56	3.92	267.23							
Mean	67.27	656.06	61.78	790.61	64.33	652.75	46.09	293.32	13.53	447.09	9.61	398.44	5.79	267.33							
Std dev	15.77	20.47	16.18	58.46	21.94	61.09	9.34	35.05	2.07	8.50	1.57	13.15	2.58	58.92							

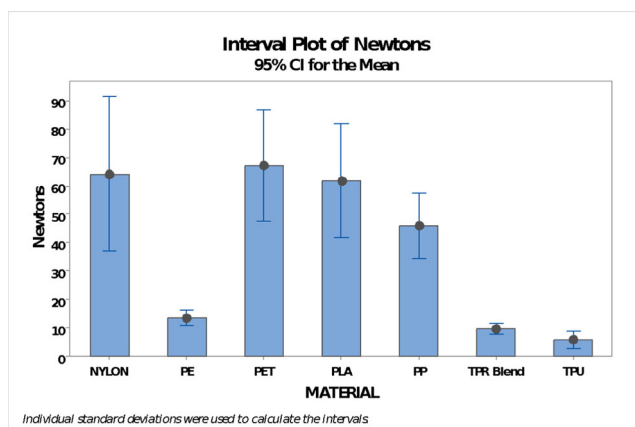


Fig. 9 Interval plot for the response of axial force before any deformation occurs

with 31.55 mm, while PE comes next with 13.41 mm. The PLA curve is related to the highest endurance with 5.9 mm of elongation, while PETG and nylon features a more characteristic curve of tough and strong plastics with an elongation of 9.2 mm and 9.4 respectively. Finally, PP (7.8 mm of elongation) featured a similar maximum load to TPU but with a substantial difference in ductility.

4.3 Fractographic analysis of folding endurance

The fracture surfaces of failed hinges were examined via scanning electron microscopy (SEM) through the use of a Hitachi SU-3500 variable pressure SEM. Surface imaging was carried out at a pressure of 80 Pa and an accelerating voltage of 10 kV. Operating the unit at 80 Pa facilitated specimen charging mitigation and allowed for fracture surface examination without the need for sputter coating. The variety of materials tested allowed for the observation of multiple fracture surface characteristics. Since no TPU specimens failed, this material system was omitted in this part of the study.

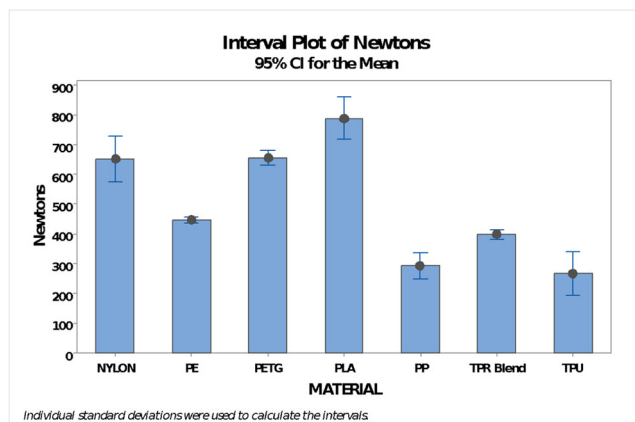


Fig. 10 Interval plot for the response of axial force to a maximum load

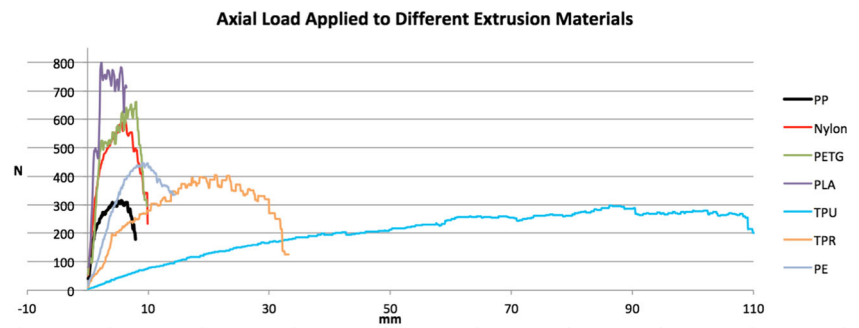
Analysis of the electron micrographs revealed that in the case of PLA and PETG the fracture morphology was dominated by characteristics consistent with dynamic fatigue. The key characteristic of fatigue failure is the presence of fatigue striations [39], a feature that was expected given the nature of our testing. The PLA micrographs (Fig. 12) revealed the striations to have grown to the point of ledge formation (highlighted by the dashed circle) and to be running roughly perpendicular to the direction of the craze crack propagation (some are indicated by the arrows). The final rupture occurred near the center of the micrograph as evident by the smooth surface.

The specimens fabricated from PETG (Fig. 13) also exhibited fatigue striations. The propagation of the craze cracking along with the curvature of the striations indicates, as was the case with PLA, that the majority of the crack growth initiated at the hinge surface and then extended inward, where final fracturing occurred within the bulk of the hinge material. Delamination at raster interfaces was also observed. The striations morphology on either side of the delamination (indicated by arrows) revealed the fracture propagation to be in opposite directions from one another, meaning the delamination occurred near the final rupture point. As was the case with PLA, the final rupture area is evident due to the smooth fracture surface.

The fracture morphology of nylon (Fig. 14) also featured fatigue striations; however, not much plastic deformation was observed on the fracture surface, nor did the striations progress to ledge formation, as was the case for PLA and PETG. In some areas of the fracture surface, there was evidence of burnishing as indicated by a smooth surface and flakes of material. Such a presence of burnishing shows that fracture in these areas occurred prior to the specimen's final breakage. Additionally, due to the printing process, a large amount of air gap between the print rasters was observed on the nylon specimens, which could have negatively influenced the mechanical properties of the printed hinges. The failure on the nylon hinge differed from the one found on the PLA and PETG hinges as the final fracture occurred at the bottom of the hinge rather than in the middle, as is indicated in Fig. 14. Crack propagation (general direction indicated by the arrow) initiated from the top (root) of the hinge and progressed rapidly as it reached the most robust printing area. The failure of the hinge progressed more slowly in this region as indicated by the fatigue striations (indicated by the dashed oval). The final fracture occurred at the base of the hinge.

While the fracture surfaces of specimens printed from PE (Fig. 15) also showed fatigue striations, the most prominent feature on the fracture surface was craze cracking, which is indicative of a brittle fracture mode. The opened craze cracks were prominent throughout the fracture surface and, in some cases, were intermixed with fatigue striations, indicating a mixed mode ductile brittle failure. Secondary crack formation

Fig. 11 Comparison of the results of the axial load test in the considered materials



was also visible in the vicinity of the fatigue striations (highlighted by the dashed circle). There are small cusp-shaped voids visible on the fracture surface (indicated by arrows), which are likely to be air gap voids from the printing process. These voids appear to have grown due to the cycling process as the voids nearer to the point of failure have opened up in comparison to those away from the point of failure. In some instances, these voids appear to have coalesced, this leading to localized delamination.

The fracture surface images from the ABS:SEBS-g-MA hinge (Fig. 16) exhibited fracture surfaces representative of fatigue. The elastomeric nature of this material did not lead to the manifestation of fatigue striations, but the presence of fibrillation on the fracture surface is representative of ductile fatigue [39]. There was also delamination evidence between print rasters as well as secondary crack formation (Fig. 16a). At some regions on the fracture surface regions, the secondary cracking propagated to the next print raster (Fig. 16b). As was the case with the other materials in this study, flakes of material on the fracture surface indicate that there was some abrasion of the fracture surface before the specimen's final failure. Additionally, there were small pores visible on the fracture surface, which were most likely air-gap voids caused by the 3D printing process.

The PP fracture surface microanalysis (Fig. 17) revealed the presence of particles within the material (indicated by the arrow). Electron dispersive spectroscopy (EDS) revealed the

particles to be composed of calcium, aluminum, and oxygen (Fig. 17b) and are potentially present as a pigment. The presence of these particles influenced the hinge's failure mode and essentially acted similar to microvoid coalescence. Secondary cracking (indicated by the dashed ellipse) was also observable on the fracture surface.

Lastly, an X-ray computed tomography (CT) test was performed to analyze the non-broken PTU hinges. A Nikon Metrology CT Inspection System XTH225ST with a $V = 180$ kV and $I = 40$ μ A was used. The number of projections was 2400, and the pixel resolution was of 30 μ m. Digital cutting of the working volume is shown in Fig. 18a–c. Results showed samples of a growing void percentage according to the number of cycles performed during the test. Percentage of voids were from 3.49% for no folding sample to 7.66% for one million and then to 9.62% for two million cycles).

Graphs in Fig. 18a–c represent the frequency of the voids, arranged by size in millimeters. Even voids in the figures appeared to increase in size from Fig. 18a–c; small voids have more density than large ones in all samples, and as is seen in Fig. 19, defects increased as the number of folding cycles rose. Similarly, larger voids seemed to increase during the test, though in less proportion (Fig. 19). Statistical data of voids and folding cycles did not provide a good model or pattern to estimate the PTU endurance behavior of the specimens considering the voids percentage.

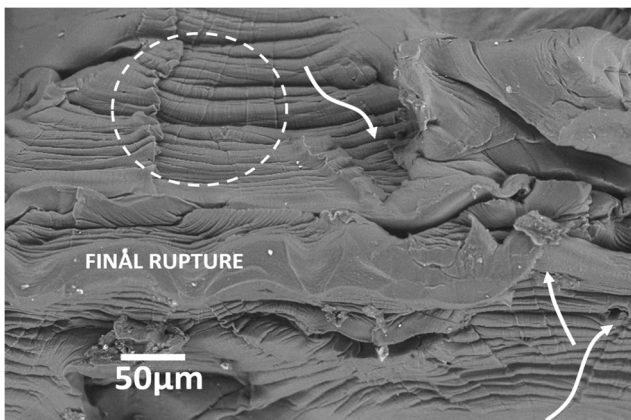


Fig. 12 SEM micrograph of the PLA fracture surface

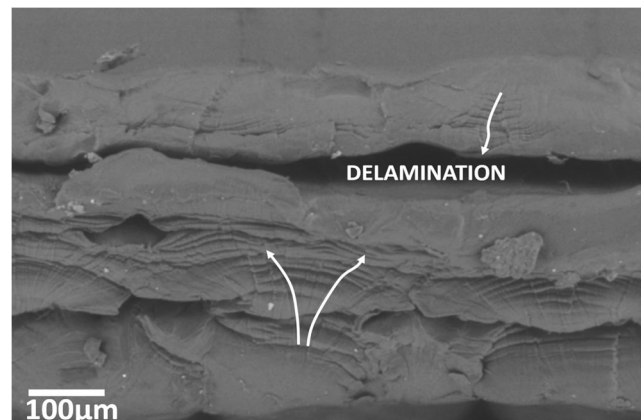


Fig. 13 SEM micrograph of the PETG fracture surface

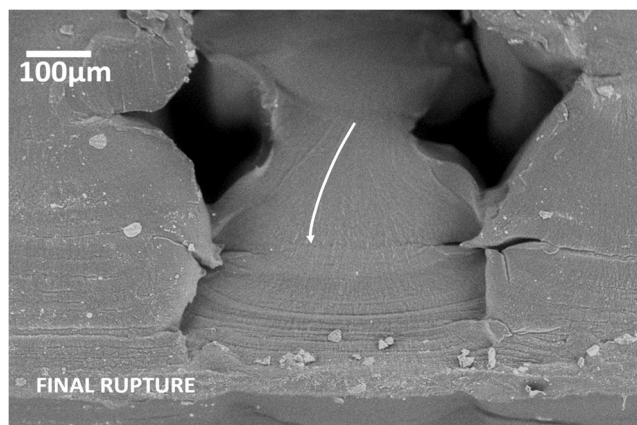


Fig. 14 SEM micrograph of the fracture surface of the hinge fabricated from nylon. Note that the final failure occurred at the base of the hinge

5 Conclusions

Thermoplastic materials used as filaments for polymer extrusion AM can be used to manufacture folding products for different applications. Although no single system was able to print all considered materials due to some of the printers' characteristics and proprietary aspects, it was possible to draw a reasonable comparison for seven materials. Pre-experiment found that best orientation to print a living hinge is XYZ considering a 0° or 45° - 45° raster angle. PLA, PE, and nylon materials are suitable for prototyping, as they require only a

few cycles of folding or the rapid manufacturing of disposable folding products such as packing with the capability to sustain axial forces of around 60 N with no deformation. PETG was shown to work for more than 800 folding cycles at 180° of flexion, considering the arithmetic mean of the hold static weight of 67.27 ± 15.77 N, with a maximum load endurance mean of 656.06 ± 20.47 N.

Three materials achieved truly flexible characteristics. The TPR blend demonstrated the potential for rapid manufacturing applications, requiring more than 240,000 folding cycles. The 3D printed PP semi-rigid material could be as effective as some traditional injection-molding for folding products which normally endure over one million cycles without rupture. In the first axial load test, PP was statistically similar to the more rigid materials mentioned in the above paragraph. TPU formulated thermoplastic polyurethane (NinjaFlex Brand) was tested for two million folding cycles without any visual damage. CT inspection of TPU revealed an increment of 6.13% in the internal voids of the folding line after two million cycles and, thus, a possible fracture with no specific prognosis in the number of folding cycles before failure. TPU could be used for applications with low axial loads or combined with rigid material inserts to provide greater endurance.

The presented failure analysis of the hinges revealed a wide variety of fracture morphologies and modes according to the hinge's material; SEM micrographs revealed pores, cracks, flakes or striations as well as colorations explaining the be-

Fig. 15 **a** SEM micrograph of the PE fracture surface showing voids and fatigue striations along with secondary crack formation. **b** Delamination along the print raster interface

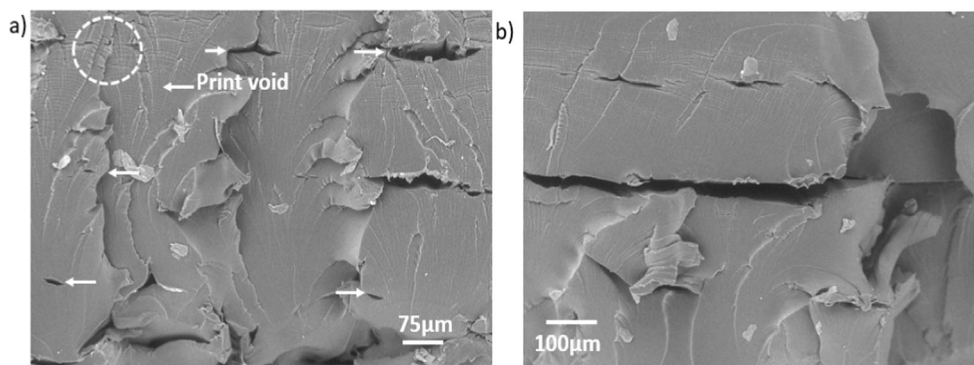


Fig. 16 **a** Electron micrograph of the fracture surface of the hinge fabricated from the blend of ABS:SEBS-g-MA exhibiting heavy delamination and secondary cracking. **b** An area where the secondary cracking propagated to the print raster interface

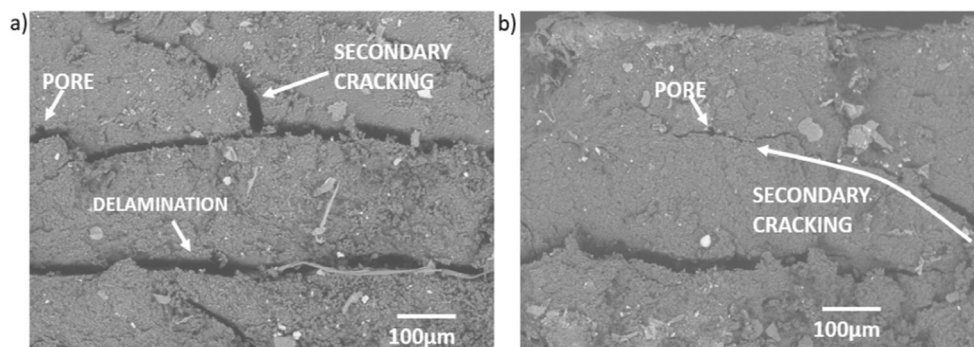


Fig. 17 **a** SEM micrograph of the PP fracture surface. **b** EDS spectra representing the composition of the observed particles

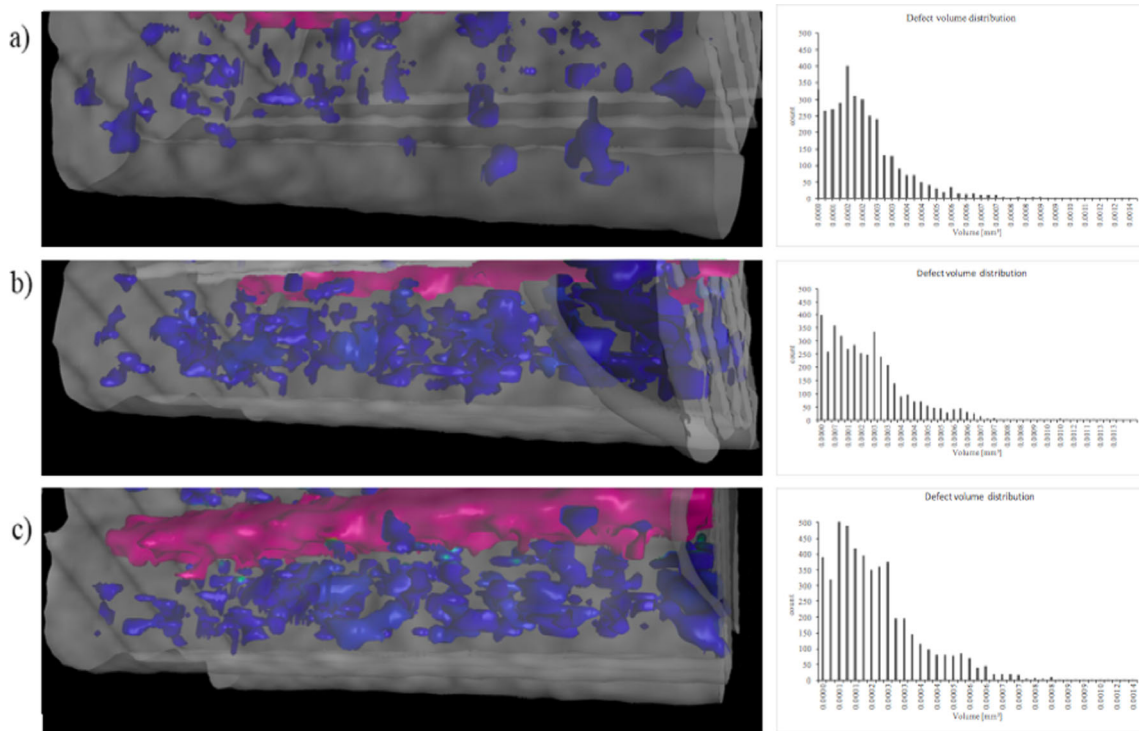
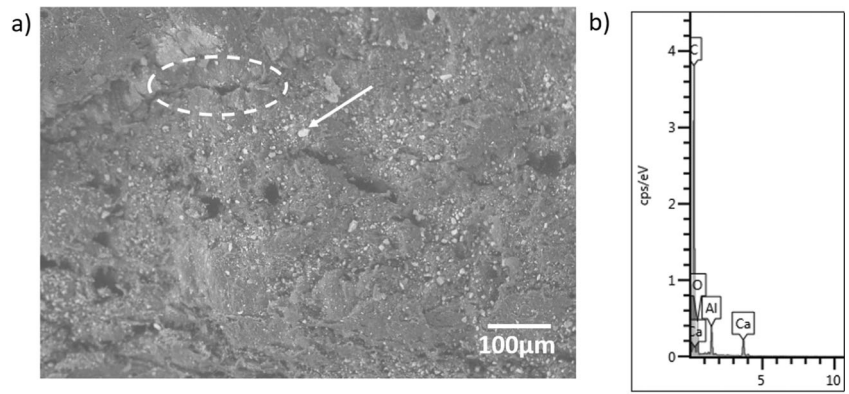
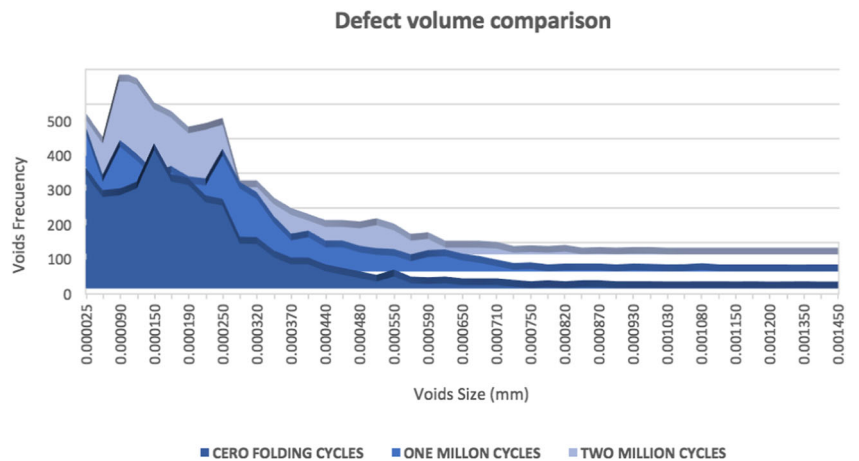


Fig. 18 **a** CT for no folding cycles hinge. **b** CT for 1 million cycles hinge. **c** CT for 2 million cycles hinge

Fig. 19 Comparison of the voids frequency according to the volume size and the number of folding cycles



havior before final failure. The work presented here provides insight into the material selection process for the 3D printing of a living hinge, which can support the development of flexible applications.

Acknowledgments The research presented here was conducted in the Rapid Prototyping Lab at the Universidad Autónoma de Ciudad Juárez (Autonomous University of Ciudad Juárez) in Collaboration with The University of Texas at El Paso (UTEP) in the W.M. Keck Center for 3D Innovation. The Friedman Chair for Manufacturing at Youngstown State University also supported the work.

Funding information Funding for this work was provided by the AFOSR through the Young Investigator Program (YIP) under grant number FA9550-14-1-0260 and the Defense University Instrumentation Program (DURIP) under grant number FA9550-15-1-0312.

References

- Melnikova R, Ehrmann A, Finsterbusch K (2014) 3D printing of textile-based structures by fused deposition modelling (FDM) with different polymer materials. *IOP Conf Ser Mater Sci Eng* 62: 012018
- Irwin MD, Roberson DA, Olivas RI, Wicker RB, MacDonald E (2011) Conductive polymer-coated threads as electrical interconnects in e-textiles. *Fibers Polym* 12:904–910
- Rocío R, Ruiz-Huerta L, Almanza-Arjona YC et al (2017) Nanocomposites for additive manufacturing. *Am J Chem Res* 1: 1–14
- Spahiu T, Piperi E, Grimmelsmann N et al (2016) 3D printing as a new technology for apparel designing and manufacturing. In: *International Textile Conference*
- MacDonald E, Wicker R (2016) Multiprocess 3D printing for increasing component functionality. *Science* 353:aaf2093. <https://doi.org/10.1126/science.aaf2093>
- Muth JT, Vogt DM, Truby RL, Mengüç Y, Kolesky DB, Wood RJ, Lewis JA (2014) Embedded 3D printing of strain sensors within highly stretchable elastomers. *Adv Mater* 26:6307–6312
- Cao Q, Kim H-S, Pimparkar N, Kulkarni JP, Wang C, Shim M, Roy K, Alam MA, Rogers JA (2008) Medium-scale carbon nanotube thin-film integrated circuits on flexible plastic substrates. *Nature* 454:495–500
- Ko SH, Pan H, Grigoropoulos CP, Luscombe CK, Fréchet JMJ, Poulidakos D (2007) All-inkjet-printed flexible electronics fabrication on a polymer substrate by low-temperature high-resolution selective laser sintering of metal nanoparticles. *Nanotechnology* 18:345202
- Ahn J-H, Kim H-S, Lee KJ, Jeon S, Kang SJ, Sun Y, Nuzzo RG, Rogers JA (2006) Heterogeneous three-dimensional electronics by use of printed semiconductor nanomaterials. *Science* 314:1754–1757
- Telfer S, Munguia J, Pallari J, Dalgamo K, Steultjens M, Woodburn J (2014) Personalized foot orthoses with embedded temperature sensing: proof of concept and relationship with activity. *Med Eng Phys* 36:9–15
- Ma RR, Odhner LU, Dollar AM (2013) A modular, open-source 3D printed underactuated hand. In: *2013 IEEE International Conference on Robotics and Automation*
- Lipson H (2014) Challenges and opportunities for design, simulation, and fabrication of soft robots. *Soft Rob* 1:21–27
- Umedachi T, Vikas V, Trimmer BA (2013) Highly deformable 3-D printed soft robot generating inching and crawling locomotions with variable friction legs. In: *2013 IEEE/RSJ International Conference on Intelligent Robots and Systems*
- Rossiter J, Walters P, Stoimenov B (2009) Printing 3D dielectric elastomer actuators for soft robotics. In: *Electroactive Polymer Actuators and Devices (EAPAD) 2009*
- Bartlett NW, Tolley MT, Overvelde JTB, Weaver JC, Mosadegh B, Bertoldi K, Whitesides GM, Wood RJ (2015) SOFT ROBOTICS. A 3D-printed, functionally graded soft robot powered by combustion. *Science* 349:161–165
- Crocco D, De Agostinis M, Olmi G (2013) Experimental characterization and analytical modelling of the mechanical behaviour of fused deposition processed parts made of ABS-M30. *Comput Mater Sci* 79:506–518
- Torrado Perez AR, Roberson DA, Wicker RB (2014) Erratum to: Fracture surface analysis of 3D-printed tensile specimens of novel ABS-based materials. *J Fail Anal Prev* 14:549–549
- Bellini A, Güçeri S (2003) Mechanical characterization of parts fabricated using fused deposition modeling. *Rapid Prototyp J* 9: 252–264
- Es-Said OS, Foyos J, Noorani R, Mendelson M, Marloth R, Pregarer BA (2000) Effect of layer orientation on mechanical properties of rapid prototyped samples. *Mater Manuf Process* 15:107–122
- Bagsik A, Schöppner V, Klemp E (2010) FDM part quality manufactured with Ultem* 9085. In: *DMRC (ed) International Science Conference Polymeric Materials*
- Torrado AR, Shemelya CM, English JD, Lin Y, Wicker RB, Roberson DA (2015) Characterizing the effect of additives to ABS on the mechanical property anisotropy of specimens fabricated by material extrusion 3D printing. *Addit Manuf* 6:16–29
- Lee CS, Kim SG, Kim HJ, Ahn SH (2007) Measurement of anisotropic compressive strength of rapid prototyping parts. *J Mater Process Technol* 187–188:627–630
- Wu W, Geng P, Li G, Zhao D, Zhang H, Zhao J (2015) Influence of layer thickness and raster angle on the mechanical properties of 3D-printed PEEK and a comparative mechanical study between PEEK and ABS. *Materials* 8:5834–5846
- Lee BH, Abdullah J, Khan ZA (2005) Optimization of rapid prototyping parameters for production of flexible ABS object. *J Mater Process Technol* 169:54–61
- Vega V, Clements J, Lam T et al (2010) The effect of layer orientation on the mechanical properties and microstructure of a polymer. *J Mater Eng Perform* 20:978–988
- Roberson DA, Torrado Perez AR, Shemelya CM, Rivera A, MacDonald E, Wicker RB (2015) Comparison of stress concentrator fabrication for 3D printed polymeric izod impact test specimens. *Addit Manuf* 7:1–11
- Balderrama-Armendariz CO, MacDonald E, Espalín D, Cortes-Saenz D, Wicker R, Maldonado-Macias A (2018) Torsion analysis of the anisotropic behavior of FDM technology. *Int J Adv Manuf Technol* 96:307–317. <https://doi.org/10.1007/s00170-018-1602-0>
- Torres J, Coteló J, Karl J, Gordon AP (2015) Mechanical property optimization of FDM PLA in shear with multiple objectives. *JOM* 67:1183–1193
- ASTM (2007) Standard test method for folding endurance of paper by the M.I.T. tester. *ASTM International*
- International Organization for Standardization (1993) Test method for folding endurance of paper by the M.I.T. tester. *ISO*
- Mraz S (2004) Care and feeding of living hinges. In: *Machine design*. <http://www.machinedesign.com/fasteners/care-and-feeding-living-hinges>. Accessed 29 May 2018
- USP (2017) Polypropylene hinge. In: *United States Plastic Corp*. <https://www.usplastic.com/search/default.aspx?it=item&keyword=Polypropylene%20Hinge>
- Siqueiros JG, Gilberto Siqueiros J, Schnitker K, Roberson DA (2016) ABS-maleated SEBS blend as a 3D printable material. *Virtual Phys Prototyp* 11:123–131

34. Meng Q, Li Y, Xu J (2013) New empirical stiffness equations for corner-filletted flexure hinges. *Mech Sci* 4:345–356
35. Dirksen F, Lammering R (2011) On mechanical properties of planar flexure hinges of compliant mechanisms. *Mech Sci* 2:109–117
36. Zhu Z, Zhou X, Wang R, Liu Q (2014) A simple compliance modeling method for flexure hinges. *Sci China Technol Sci* 58: 56–63
37. Smyth CT (2017) *Functional design for 3D printing: designing 3D printed things for everyday use*, 3rd edn
38. ASTM Committee F42 on Additive Manufacturing Technologies, ASTM Committee F42 on Additive Manufacturing Technologies. Subcommittee F42.01 on Test Methods, Technical Committee ISO/TC 261, Additive Manufacturing (2013) Standard terminology for additive manufacturing—coordinate systems and test methodologies
39. Engel L (1981) *An atlas of polymer damage: surface examination by scanning electron microscope*, Wiley-Blackwell

Publisher's note Springer Nature remains neutral with regard to jurisdictional claims in published maps and institutional affiliations.

Terms and Conditions

Springer Nature journal content, brought to you courtesy of Springer Nature Customer Service Center GmbH (“Springer Nature”).

Springer Nature supports a reasonable amount of sharing of research papers by authors, subscribers and authorised users (“Users”), for small-scale personal, non-commercial use provided that all copyright, trade and service marks and other proprietary notices are maintained. By accessing, sharing, receiving or otherwise using the Springer Nature journal content you agree to these terms of use (“Terms”). For these purposes, Springer Nature considers academic use (by researchers and students) to be non-commercial.

These Terms are supplementary and will apply in addition to any applicable website terms and conditions, a relevant site licence or a personal subscription. These Terms will prevail over any conflict or ambiguity with regards to the relevant terms, a site licence or a personal subscription (to the extent of the conflict or ambiguity only). For Creative Commons-licensed articles, the terms of the Creative Commons license used will apply.

We collect and use personal data to provide access to the Springer Nature journal content. We may also use these personal data internally within ResearchGate and Springer Nature and as agreed share it, in an anonymised way, for purposes of tracking, analysis and reporting. We will not otherwise disclose your personal data outside the ResearchGate or the Springer Nature group of companies unless we have your permission as detailed in the Privacy Policy.

While Users may use the Springer Nature journal content for small scale, personal non-commercial use, it is important to note that Users may not:

1. use such content for the purpose of providing other users with access on a regular or large scale basis or as a means to circumvent access control;
2. use such content where to do so would be considered a criminal or statutory offence in any jurisdiction, or gives rise to civil liability, or is otherwise unlawful;
3. falsely or misleadingly imply or suggest endorsement, approval, sponsorship, or association unless explicitly agreed to by Springer Nature in writing;
4. use bots or other automated methods to access the content or redirect messages
5. override any security feature or exclusionary protocol; or
6. share the content in order to create substitute for Springer Nature products or services or a systematic database of Springer Nature journal content.

In line with the restriction against commercial use, Springer Nature does not permit the creation of a product or service that creates revenue, royalties, rent or income from our content or its inclusion as part of a paid for service or for other commercial gain. Springer Nature journal content cannot be used for inter-library loans and librarians may not upload Springer Nature journal content on a large scale into their, or any other, institutional repository.

These terms of use are reviewed regularly and may be amended at any time. Springer Nature is not obligated to publish any information or content on this website and may remove it or features or functionality at our sole discretion, at any time with or without notice. Springer Nature may revoke this licence to you at any time and remove access to any copies of the Springer Nature journal content which have been saved.

To the fullest extent permitted by law, Springer Nature makes no warranties, representations or guarantees to Users, either express or implied with respect to the Springer nature journal content and all parties disclaim and waive any implied warranties or warranties imposed by law, including merchantability or fitness for any particular purpose.

Please note that these rights do not automatically extend to content, data or other material published by Springer Nature that may be licensed from third parties.

If you would like to use or distribute our Springer Nature journal content to a wider audience or on a regular basis or in any other manner not expressly permitted by these Terms, please contact Springer Nature at

onlineservice@springernature.com